PHOTONIC SENSORS / Vol. 16, No. 1, 2026: 9560003

In-Situ Identification and Concentration Detection of Microfluidic Liquid Using a Non-Contact Photoacoustic Sensing Approach

Liheng YANG[1,2], Dian MIAO[1], Yu WANG[1], Zewen HAN[1], Xi YANG[1,3], Xiaoxiao CHEN[4], Shigui XUE[5], Mateusz SMIETANA[6], Yuan GONG[1*], and Yunjiang RAO[1]

[1]*Key Laboratory of Optical Fiber Sensing and Communications (Ministry of Education of the People's Republic of China), University of Electronic Science and Technology of China, Chengdu 611731, China*

[2]*National Center (Sichuan) of Technology Innovation for Advanced Aviation Equipment Corporation, Chengdu 610074, China*

[3]*Frontiers Science Center for Nano-Optoelectronics and State Key Laboratory for Mesoscopic Physics, School of Physics, Peking University, Beijing 100871, China*

[4]*Institute of Optics, National Institute of Measurement and Testing Technology, Chengdu 610021, China*

[5]*Sinopec Key Laboratory of Geophysics, Sinopec Geophysical Research Institute Co., Ltd., Nanjing 211103, China*

[6]*Institute of Microelectronics and Optoelectronics, Warsaw University of Technology, Koszykowa 75, Warsaw 00-662, Poland*

[*]Corresponding author: Yuan GONG E-mail: ygong@uestc.edu.cn

Abstract: Microfluidic liquid samples are crucial in both biomedical and chemical engineering, however, their in-situ identification and testing remain a major challenge. Here, we developed a non-contact photoacoustic (PA) sensor for in-situ and real-time identification and concentration detection of substances in a microfluidic environment. The ultrasonic vibration of the microfluidic samples was generated by a free-space pulsed laser pump and detected by a non-contact laser Doppler vibrometer. The time- and frequency-domain responses of the PA signals were employed to achieve substance identification and concentration detection. Principal component analysis (PCA) and adaptive boosting (AdaBoost) algorithms were employed to extract the frequency-domain characteristics, and an identification accuracy of over 98% was achieved. Chemical samples down to the nanomolar (nM) level can be detected by analyzing either the time-domain or frequency-domain response. The proposed sensor with non-contact and fast detection provides a promising platform for in-situ and real-time monitoring of samples in microfluidic systems.

Keywords: Photoacoustic effect; chemical sensor; microfluidics; substance identification; concentration detection.

Citation: Liheng YANG, Dian MIAO, Yu WANG, Zewen HAN, Xi YANG, Xiaoxiao CHEN, *et al*., "In-Situ Identification and Concentration Detection of Microfluidic Liquid Using a Non-Contact Photoacoustic Sensing Approach," *Photonic Sensors*, 2026, 16(1): 9560003.

Received: 27 September 2025 / Revised: 27 November 2025

DOI: 10.26599/PhoS.2026.9560003
Article type: Research article

1. Introduction

Photoacoustic (PA) sensing holds considerable promise in biomedical diagnostics, industrial safety, and gas detection applications [1, 2]. Optical absorption of a modulated or pulsed laser leads to heat production in samples and generation of acoustic waves. The PA spectroscopy (PAS) enables identification of different substances and detection of their concentration [3–8]. However, the acquisition of PA fingerprint spectra involves wavelength scanning, which significantly limits the efficiency of applications [8–10].

In addition to efficient acoustic generation, the performance of a PA sensor is highly dependent on the acoustic detection methodology. Quartz tuning forks (QTFs) have been utilized as a key technology for acoustic detection, providing high sensitivity due to their resonant properties and being widely used in low-damping gas detection applications [10–13]. In high-damping environments, such as liquids, electrical microphones based on piezoelectric and microelectromechanical system (MEMS) sensors are typically used to detect acoustic waves [14, 15]. To further enhance sensitivity, novel detection technologies, such as optical microcavities and other types of optical sensors, have been extensively explored. Optical microcavities, such as the Fabry-Pérot cavity and whispering-gallery mode cavity with ultrahigh quality factors, effectively improve the signal-to-noise ratio (SNR) for PA sensing [16–21]. Optical microphones employ micro- or nano-structures to amplify and detect vibrations caused by acoustic waves. Representative examples include micro-interferometric or micro-laser-based sensors integrated with silicon cantilevers or membranes, which facilitate highly sensitive PA detection [22–26]. These detection methods rely on acoustic impedance matching or the direct contact between the sensor and the liquid medium to achieve high sensitivity. Such requirements limit the applicability of the method to tight-space environments, such as microfluidic chips, in which invasive detection and sample contamination are unacceptable.

To address the above limitations, we report a non-contact PA sensor for real-time substance identification and concentration detection (Fig. 1). A pulsed laser and a non-contact laser Doppler vibrometer (LDV) were employed to achieve the generation and detection of acoustic waves, respectively. Substance identification was achieved by analyzing the frequency characteristics of PA signals with principal component analysis (PCA) and adaptive boosting (AdaBoost) algorithms. The intensity of PA signals from the chemical samples quantitatively reflects their concentrations. The identification of six chemical samples was demonstrated experimentally, including two types of solutions and four types of suspensions. The identification accuracy exceeded 98%. The limit of detection (LOD) reached the nanomolar (nM) level for the rhodamine B (RhB) solution. In addition, this approach overcomes the limitations of optical refractive index sensors where distinguishing different types of samples is challenging. We anticipate that it will find applications in non-invasive liquid detection.

2. Experimental setup and principle

2.1 Experimental setup

The schematic diagram of the non-contact PA sensor is shown in Fig. S1. A 532 nm pulsed laser (Dawa-200; Beamtech Optronics Co., Ltd., China; 20 μm spot diameter; 20 Hz repetition rate) was used to stimulate the chemical sample in a microfluidic channel (see S1, Supplementary files for more details). Due to the thermoelastic and vaporization effects (see S2, Supplementary files for more details), microbubbles were formed and ultrasonic waves were efficiently generated within the liquid sample. The ultrasonic waves induced vibrations in the liquid and also on the surface of the microfluidic channel, which was detected by an

LDV. The LDV (OFV-505/5000, Polytec Ltd., Germany) offered a velocity resolution of 20 mm/s/V with a bandwidth of 1 MHz. It is a non-contact detection method with a signal delay of microseconds, enabling real-time PA detection. Both the pump laser and the probe laser were co-aligned through an objective to enhance the efficiency for both the pump and probe. A charge-coupled device (CCD) was used to monitor the focusing of both the pump and detection beams in real time. The pump laser pulse was used as a trigger for the LDV to record the PA signal. The free-space pump and detection configuration made it possible to avoid sample contamination and was available for in-situ monitoring of microfluidic systems. The LDV-based PA sensor featured fast and non-contact detection, promoting its applications for in-situ and real-time detection of liquid substances.

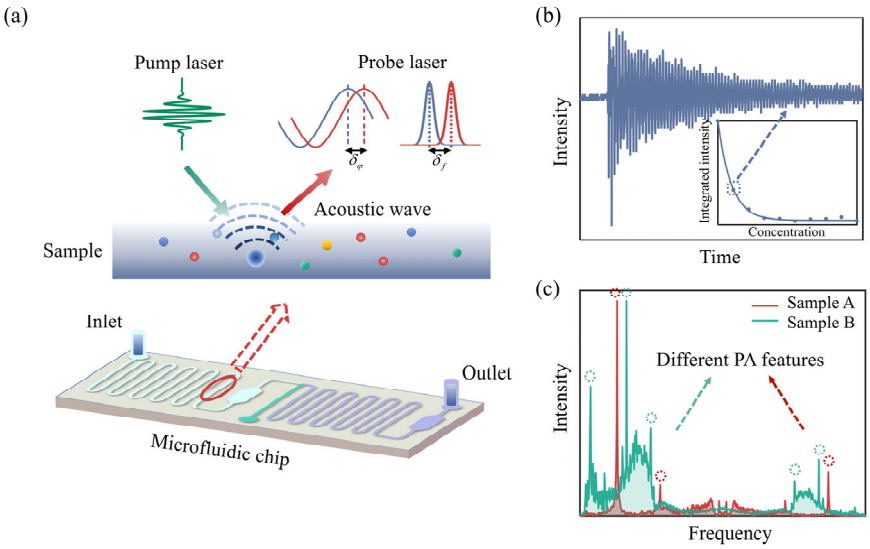

Fig. 1 Non-contact PA sensor for microfluidic analysis: (a) schematic of the PA sensor, (b) typical PA signals in the time domain, and (c) in the frequency domain.

2.2 Characterization of the non-contact PA sensor

The time-domain PA signals acquired at different pump energy for water are illustrated in Fig. 2(a). The PA signal highly depended on the pump laser energy. In the low pump energy region [Region I, <80 μJ for water, Fig. 2(b)], no PA signals were excited. With the increasing pump energy (Region II, 80 μJ–90 μJ for water), a weak PA signal emerged due to the thermoelastic-induced ultrasonic waves. The turning point from Region I to Region II was defined as the threshold for the PA signal, which depended on the optical absorption coefficient and photothermal conversion coefficient of the sample. When the pump energy was high (Region III, >90 μJ for water), the vaporization of liquid led to the formation of microbubbles to generate an intense vibration, boosting the PA signal. The transition from Region II to Region III relied on the boiling point of the liquid. The evolution of microbubbles is illustrated in Fig. S2. In addition, ionization glow [27] was not observed in our experiments due to the energy limitations of the pump laser.

Similar phenomena were observed and three regions could be distinguished for other samples [Fig. 2(b) for methanol, ethanol, and the mixture of ethanol and water, and Fig. S3 for the six samples to be tested]. Since the boiling point of ethanol (78.3 ℃) is lower than that of water under the standard atmospheric pressure, the threshold for transition from Region II to III was reduced from 90 μJ to 50 μJ. The threshold for the ethanol-water mixture was between those of pure water and ethanol. With a further decrease in the boiling point (methanol, 64.7 ℃), the threshold showed a proportional reduction (Fig. S4).

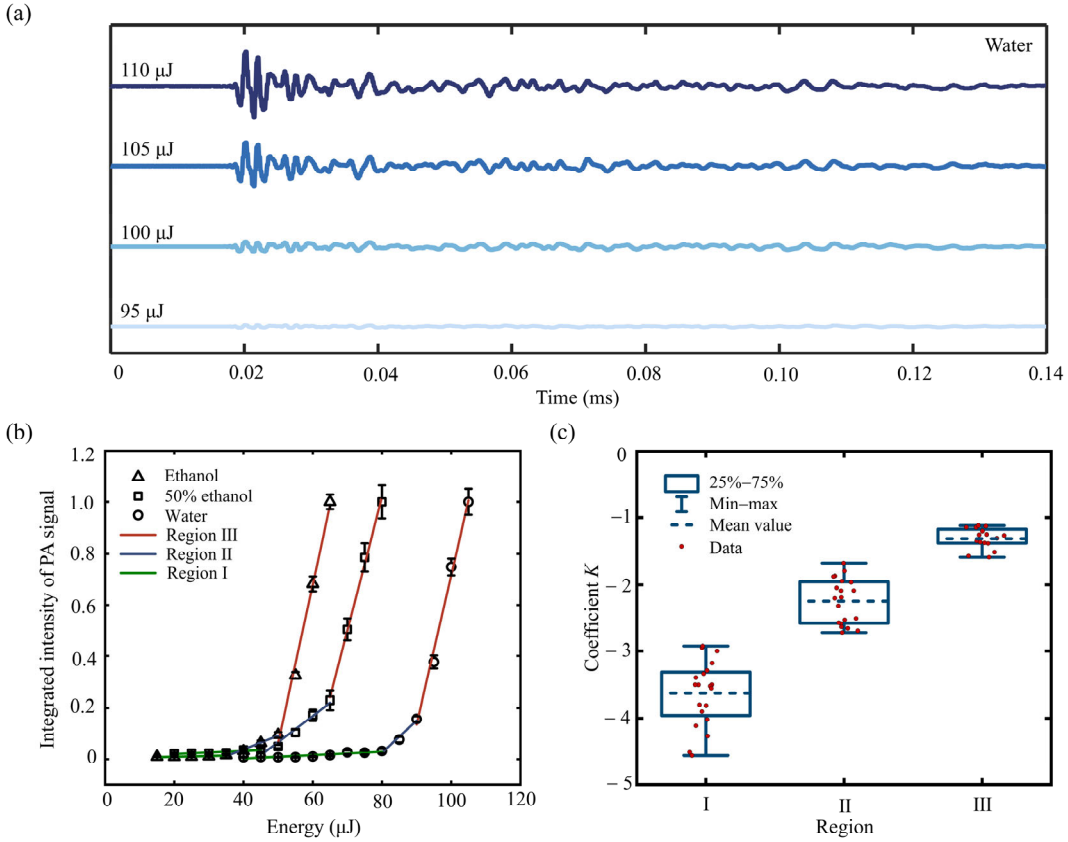

Fig. 2 Characterization of non-contact PA sensor: (a) time-domain PA signals of water at different pump energy, (b) normalized integrated intensity of PA signals in the time domain of water, ethanol, and 50% ethanol in water as a function of pump energy, and (c) statistics of the coefficient K in various regions.

To distinguish the three regions, a coefficient K is defined as

$$K = \lg\left(I/E_L\right) \tag{1}$$

where I is the integrated intensity of the PA signals and E_L is the energy of the pump laser. Various K values corresponded to Regions I, II, and III, respectively [Fig. 2(c)]. In Region II, the PA signals offered smaller error bars than in Region III [Figs. 2(b), S3, and S4], which indicated strong stability and repeatability that could effectively enhance the accuracy of the measurement. In contrast, the PA effect in Region III was more evident, and the PA signals were highly affected by the microbubbles as the laser energy increased, resulting in relatively larger error bars [Figs. 2(b), S3, and S4]. The measurement accuracy might degrade due to the decreased signal stability, although extremely strong PA signals were obtained. Therefore, substance identification and concentration detection were optimally performed in Region II, while Region III remained acceptable. In the experiments, the pump laser energy was selected according to the SNR and stability of PA signals, which primarily determined the precision and reliability of the sensor.

3. Experimental results

3.1 Substance identification

Multi-parameter sensing [28] and multi-analyte identification [1] are critical in the various scenarios. We chose various liquids in the microfluidic system to demonstrate the ability of the non-contact PA sensor for substance identification, including the solutions of RhB, fluorescent product (FP) resulted from horseradish peroxidase-substrate reaction, and the suspensions of polymer microspheres (PS), magnetic beads (MB), multi-walled carbon

nanotubes (MWCNTs), and gold nanoparticles (AuNPs). The absorption spectra (Fig. S5) and size information (Fig. S6) are described in S5, Supplementary file. The PA signals in the time and frequency domains for these liquids are shown in Fig. 3. Comparative analysis revealed that different liquids had distinct features of PA signals in their frequency spectra under specific experimental conditions, which provided favorable conditions for substance identification. As the recording of spectra in the ultrasonic frequency domain was much faster than that of PA spectra by scanning the wavelength of the pump laser, our method is capable of real-time identification of substances.

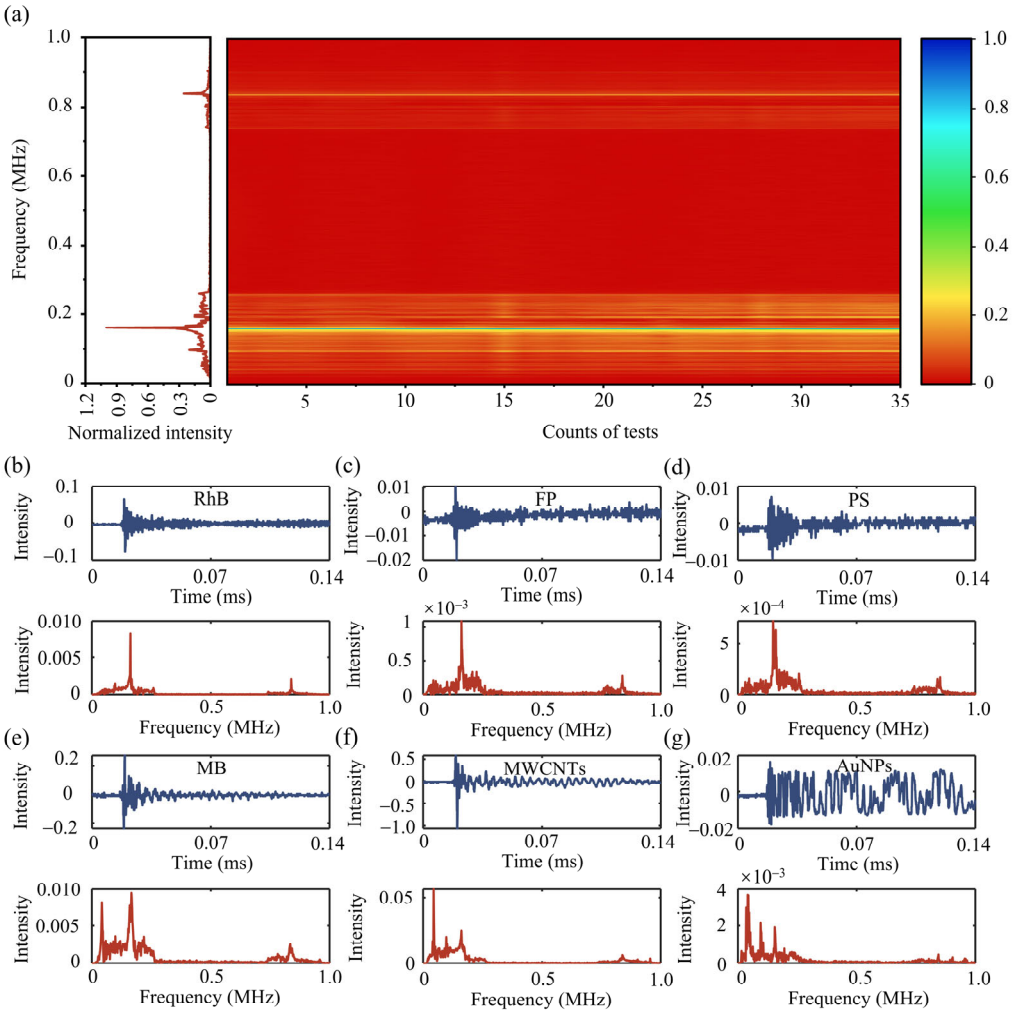

Fig. 3 Detection of six representative chemical samples using the non-contact PA sensor: (a) the repeatability of the frequency spectra of PA signals for RhB solution, (b)–(g) the time-domain signals and frequency-domain spectra of PA signals for the six samples.

3.1.1 Pump optimization

The pump energy has a significant impact on the SNR of the PA signals. Hence, the time-domain PA signals of the six substances were investigated under different pump energy (Fig. S3). The intensity is normalized for comparison. Note that the pump energy thresholds greatly depend on the analyzed sample due to its physical properties, as discussed in Section 2 (see S3 and S4, Supplementary files for more details). To achieve substance identification with a stable PA signal and high SNR, the pump energy was set at 50 μJ. We characterized their time-domain PA signals by repeating the measurement 35 times, and their frequency-domain

PA signals were obtained by calculating the corresponding Fourier transform. As shown in Fig. 3(a), the frequency spectra of RhB display multiple characteristic peaks, and all of them show excellent repeatability and stability. The photobleaching of RhB had a negligible effect on the PA signal (Fig. S7). These characteristic peaks were dominated by both the physical properties of the substance and the boundary conditions of the microfluidic channel (Fig. S8). The detailed analysis is illustrated in S7, Supplementary files. Specific frequency peaks of PA signals were observed for each of the microfluidic samples [Figs. 3(b)–3(g), S8, and S9].

3.1.2 Frequency spectra analysis based on machine learning

Initially, we attempted to classify the samples based on the two predominant peaks in the frequency spectra. However, the intricate peaks in the frequency spectra made the data analysis challenging. It was found that different substances showed an overlapped distribution and lack of clear separation boundaries [Fig. 4(a)], making it difficult to distinguish these samples. Then, the PCA algorithm was employed to achieve dimensionality reduction on the frequency spectra, retaining the two principal components with the maximum variance [29]. The detailed methods are described in S9, Supplementary files [Fig. S10(b)]. These two components were linear combinations of the original spectral components. The PCA algorithm could significantly enhance the discriminability among substances, with well-defined classification margins in the transformed feature space [Fig. 4(b)].

Further, the AdaBoost algorithm was applied to identify the type of samples [30]. The schematic diagram of AdaBoost for identification is illustrated in Fig. 4(c) and the detailed principle of AdaBoost is

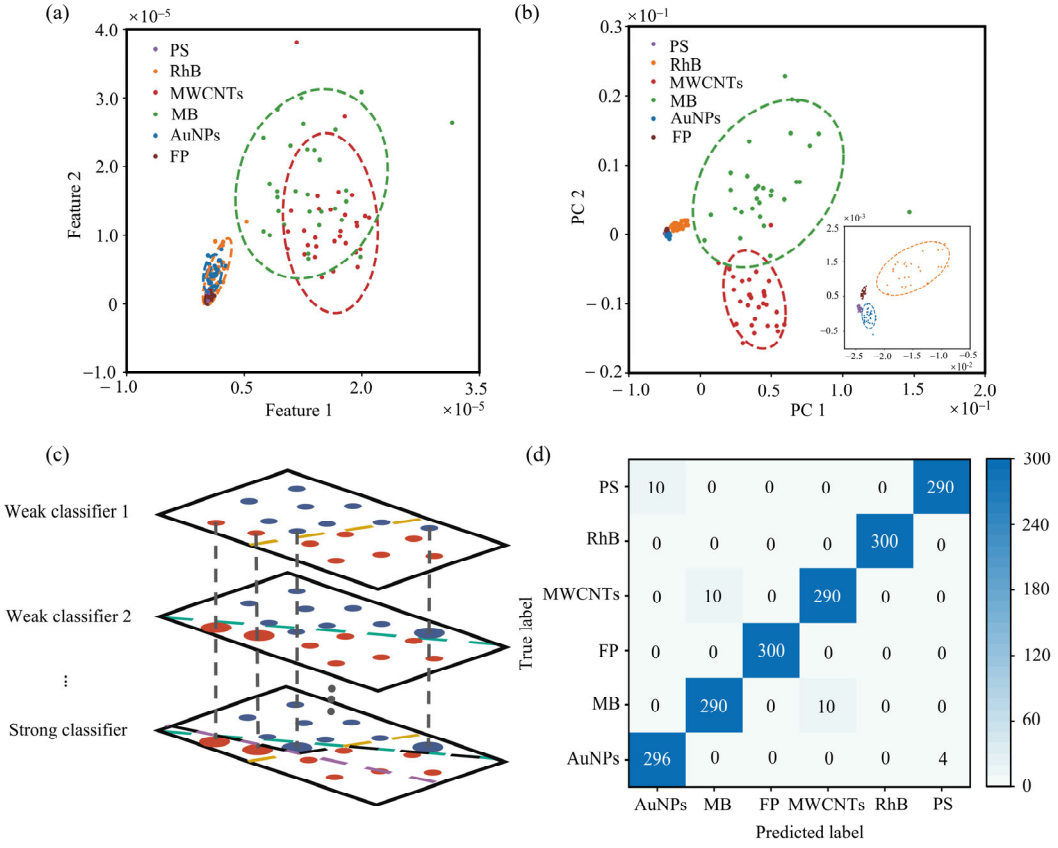

Fig. 4 Identification of six microfluidic samples: the classification of different substances (a) before and (b) after applying the principal component analysis algorithm, (c) the schematic diagram of the adaptive boosting (AdaBoost) algorithm, and (d) the confusion matrix for the combination of PCA and AdaBoost algorithms.

illustrated in S9, Supplementary files [Fig. S10(c)]. We allocated 90% of the data as the training set to train the AdaBoost model and 10% as the testing set to evaluate its identification performance. During the training process, we used five decision trees as base learners, with a maximum depth of three layers for each tree. Each decision tree assigned higher weights to the samples misclassified by the previous decision tree. The identification result of the combination of the AdaBoost with the PCA model is shown in Fig. 4(d), with an average identification accuracy exceeding 98%. By combining with the PCA algorithm, the identification accuracy for AdaBoost was improved from 89% to 98%, which is better than other machine learning algorithms (Fig. S11 and Table S1). The detailed description is illustrated in S10, Supplementary files. When the substances exhibited similar physical properties under a 532 nm pump laser, resulting in PA signals of comparable intensity and spectral features, this might lead to a reduction in identification accuracy. This problem can be further improved by using multiple pump lasers at different wavelengths to enlarge the absorption difference among the samples and to enhance the identification capability.

3.2 Detection of concentration

Next, we focused on the demonstration of the capability of the non-contact PA sensor for concentration detection. The RhB solution was used as an example for proof-of-concept. The RhB solutions with a serial dilution from 0.1 mM to 6.4 nM were prepared, and the pump energy was set at 50 μJ. Typical PA signals in the time and frequency domains for different concentrations are shown in Figs. 5(a) and 5(b). Each time-domain signal exhibited a slow damping and was highly repeatable. The characteristic peaks in the frequency spectra were stable, and the corresponding intensity increased at a higher concentration. It was attributed to the stronger absorption of the higher concentration RhB solution, enhancing the thermoelastic expansion to generate stronger PA signals. The dependence of integrated PA signals on the RhB concentration is presented in Fig. 5(c). Both

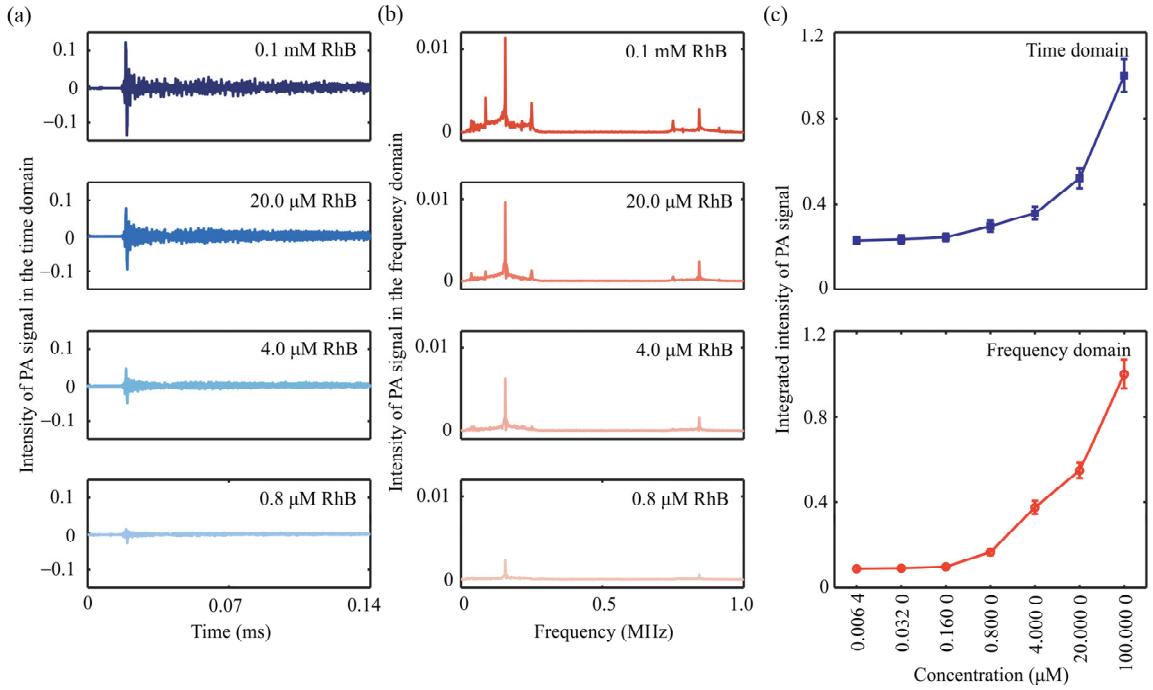

Fig. 5 Concentration detection of microfluidic samples: (a) the time-domain and (b) frequency-domain PA signals of the RhB solution with different concentrations, and (c) the calibration curves for the concentration detection of the RhB solution using the PA signals in the time domain and frequency domain.

signals in the time domain and frequency domain can be employed as a calibration curve for concentration detection. The LOD of the RhB solution is calculated to be 300 nM in the time- and frequency-domain PA signals. The concentrations of other samples were also detected with an LOD at the nM level (Figs. S12 and S13). The sensitivity of the proposed method can be further improved by the existing enhancement methods, including combining with soft materials [18, 26] and reflection enhancement membranes [31, 32].

4. Discussion

The experimental results show that the proposed non-contact PA sensor can be used for accurate substance identification and quantitative concentration detection, especially for in-situ monitoring. Compared with the chromatographic, mass spectrometric analysis, and PAS based on pump wavelength scanning [7–10, 33], this machine-learning-assisted PA sensor can identify the microfluidic samples within microseconds in the single measurement. It does not require the use of the coupling agents or any acoustic impedance matching that is essential for microphones [14–26, 34, 35]. The LDV utilizes laser interference to detect the acoustic vibration in a non-contact way, making the contamination-free analysis possible. Other non-PA sensors, such as fiber-optic surface plasmon resonance, fiber gratings, and interferometers [36–38], often need to contact the microfluidic samples that may cause the contamination or disturbance of the microfluidic systems. Many optical sensors are based on the detection of refractive index changes, which makes it difficult to distinguish different types of microfluidic samples. In addition, this method can readily be extended to other scenarios with limited spaces to achieve in-situ detection. Therefore, the LDV-based non-contact PA sensor, with its rapid response, non-contact nature, and high sensitivity, shows great promise for a wide range of applications.

Several strategies may be adopted in future work to analyze a mixture of samples. First, multiple pump lasers with different wavelengths can be employed to distinguish substances with overlapping PA spectra at one wavelength. The pump energy could be adapted for each sample to generate PA signals with a high single-to-noise ratio and also to avoid the instability caused by large bubbles. Second, a broader set of reference substances, including both pure compounds and well-designed mixtures, can be utilized to build a comprehensive PA signature database, supporting supervised learning or lookup-based identification and improving generalization to unknown substances. Third, advanced machine learning methods [39, 40] could be explored to achieve accurate identification and quantitative analysis of complex substances, such as tumor tissues.

5. Conclusions

We have developed a machine-learning-assisted PA sensing approach for non-contact, in-situ, and real-time liquid identification and concentration detection in a microfluidic system. The PA signals from thermoelastic and vaporization effects have been studied experimentally. The features of the frequency-domain PA signals were extracted through the principal component analysis algorithm to classify different samples and through the adaptive boosting algorithm to identify their types, showing identification accuracy of 98%. The concentration of the identified samples was measured by the integrated intensity of PA signals, achieving a limit of detection at the nM level. The non-contact PA sensor with a free-space pump and detection enables in-situ detection and avoids sample contamination, paving the way for online analysis of samples in microfluidic chips.

Supplementary files

The supplementary files can be downloaded from the webpage of this article in Photonic Sensors (https://www.sciopen.com/journal/1674-9251).

Acknowledgment

This work was supported by the National Key R&D Program of China (Grant No. 2023YFB2806702); the National Natural Science Foundation of China (Grant Nos. 62275043 and 62205007); the National Center of Technology Innovation for Advanced Aviation Equipment Science Foundation, China (Grant No. 010601012514); the Central Government-Guided special fund for Local Science and Technology Development Project, China (Grant No. 2024ZYD0254); the Fundamental Research Funds for the Central Universities, China (Grant No. ZYGX2025XJ006); the Exchange Project for Key Lab of Optical Fiber Sensing and Communications (Ministry of Education of the People's Republic of China) (Grant No. ZYGX2024K010).

Declarations

Conflict of Interest Yunjiang RAO is the editor-in-chief for Photonic Sensors. He was not involved in the editorial review, or the decision to publish this article. All authors declare that there are no competing interests.

Use of AI Statement None.

References

[1] Q. Wei, B. Li, B. Zhao, and Y. Wang, "Highly sensitive photoacoustic multi-gas detection of SF_6 decomposition components," *Photonic Sensors*, 2025, 15(4): 250430.

[2] G. Wissmeyer, M. A. Pleitez, A. Rosenthal, and V. Ntziachristors, "Looking at sound: optoacoustics with all-optical ultrasound detection," *Light: Science & Applications*, 2018, 7(1): 53.

[3] T. Schmid, C. Helmbrecht, C. Haisch, U. Panne, and R. Niessner, "On-line monitoring of opaque liquids by photoacoustic spectroscopy," *Analytical and Bioanalytical Chemistry*, 2003, 375(8): 1130–1135.

[4] M. A. Pleitez, T. Lieblein, A. Bauer, O. Hertzberg, H. von Lilienfeld-Toal, and W. Mäntele, "In vivo noninvasive monitoring of glucose concentration in human epidermis by mid-infrared pulsed photoacoustic spectroscopy," *Analytical Chemistry*, 2012, 85(2): 1013–1020.

[5] J. Laufer, D. Delpy, C. Elwell, and P. Beard, "Quantitative spatially resolved measurement of tissue chromophore concentrations using photoacoustic spectroscopy: application to the measurement of blood oxygenation and haemoglobin concentration," *Physics in Medicine and Biology*, 2006, 52(1): 141–168.

[6] M. Li, M. Hu, H. Zhang, J. Wang, T. Tang, M. Hu, *et al.*, "All-fiber photoacoustic gas sensing with interferometric location," *Photonics*, 2022, 9(8): 546.

[7] J. Liao, M. Adolphson, H. Li, D. K. Sikder, C. Lu, and L. Yang, "Whispering-gallery-mode resonators for detection and classification of free-flowing nanoparticles and cells through photoacoustic signatures," *Light: Science & Applications*, 2025, 14(1): 397.

[8] Z. Wang, J. Chang, H. Yu, C. Tian, H. Zhang, X. Zhang, *et al.*, "Multi-component and multi-point trace gas sensing in wavelength modulation spectroscopy based on wavelength stabilization," *Photonic Sensors*, 2019, 9(4): 376–387.

[9] Z. Meng, J. Zhang, J. Xiang, W. Li, L. Xia, and W. Guo, "A fast measurement method based on linearly swept wavelength modulation and frequency tracking demodulation for photoacoustic spectroscopy," *Journal of Lightwave Technology*, 2024, 42(18): 6531–6539.

[10] J. B. Christensen, L. Høgstedt, S. M. M. Friis, J. Y. Lai, M. H. Chou, D. Balslev-Harder, *et al.*, "Intrinsic spectral resolution limitations of QEPAS sensors for fast and broad wavelength tuning," *Sensors*, 2020, 20(17): 4725.

[11] S. Qiao, Y. He, H. Sun, P. Patimisco, A. Sampaolo, V. Spagnolo, *et al.*, "Ultra-highly sensitive dual gases detection based on photoacoustic spectroscopy by exploiting a long-wave, high-power, wide-tunable, single-longitudinal-mode solid-state laser," *Light: Science & Applications*, 2024, 13(1): 100.

[12] J. Wang, H. Wu, A. Sampaolo, P. Patimisco, V. Spagnolo, S. Jia, *et al.*, "Quartz-enhanced multiheterodyne resonant photoacoustic spectroscopy," *Light: Science & Applications*, 2024, 13(1): 77.

[13] H. Sun, S. Qiao, Y. He, X. Sun, and Y. Ma, "Parts-per-quadrillion level gas molecule detection: CO-LITES sensing," *Light: Science & Applications*, 2025, 14(1): 180.

[14] H. Kim, S. Yu, and S. Cho, "Detection of pressure waves in water by using optical techniques," *Journal*

of the Korean Physical Society, 2008, 53(4): 1906–1909.

[15] K. Roy, A. Kumar, V. Shastri, I. Munjal, K. Kalyan, and A. Ashok, "PMUT-powered photoacoustic detection: revolutionizing microfluidic concentration measurements," *IEEE Transactions on Instrumentation and Measurement*, 2024, 73: 1–8.

[16] S. J. Tang, M. Zhang, J. Sun, J. W. Meng, X. Xiong, Q. Gong, *et al*., "Single-particle photoacoustic vibrational spectroscopy using optical microresonators," *Nature Photonics*, 2023, 17(11): 951–956.

[17] X. Ren, J. Pan, M. Yan, J. Sheng, C. Yang, Q. Zhang, *et al*., "Dual-comb optomechanical spectroscopy," *Nature Communications*, 2023, 14(5037).

[18] X. Cao, H. Yang, Z. L. Wu, and B. B. Li, "Ultrasound sensing with optical microcavities," *Light: Science & Applications*, 2024, 13(1): 159.

[19] J. A. Guggenheim, J. Li, T. J. Allen, R. J. Colchester, S. Noimark, O. Ogunlade, *et al*., "Ultrasensitive plano-concave optical microresonators for ultrasound sensing," *Nature Photonics*, 2017, 11(11): 714–719.

[20] Z. Wang, Q. Nie, H. Sun, Q. Wang, S. Borri, P. D. Natale, *et al*., "Cavity-enhanced photoacoustic dual-comb spectroscopy," *Light: Science & Applications*, 2024, 13(1): 11.

[21] G. Frigenti, L. Cavigli, F. Ratto, S. Centi, T. García-Fernández, and D. Farnesi, "Microbubble resonators for photoacoustic detection and photothermal spectroscopy," *Journal of Lightwave Technology*, 2023, 41(13): 4137–4144.

[22] T. A. La, O. Ülgen, R. Shnaiderman, and V. Ntziachristos, "Bragg grating etalon-based optical fiber for ultrasound and optoacoustic detection," *Nature Communications*, 2024, 15(1): 7521.

[23] Y. Liang, H. Sun, L. Cheng, L. Jin, and B. O. Guan, "High spatiotemporal resolution optoacoustic sensing with photothermally induced acoustic vibrations in optical fibres," *Nature Communications*, 2021, 12(1): 4139.

[24] J. Ma, E. Fan, H. Liu, Y. Zhang, C. Mai, X. Li, *et al*., "Microscale fiber photoacoustic spectroscopy for in situ and real-time trace gas sensing," *Advanced Photonics*, 2024, 6(6): 066008.

[25] X. Zhao, H. Qi, Z. Wang, F. Ma, C. Li, M. Guo, *et al*., "Cantilever enhanced fiber-optic photoacoustic microprobe for diffusion detection of sulfur dioxide," *Sensors and Actuators B: Chemical*, 2024, 405: 135340.

[26] G. Wu, J. Xing, Z. Gong, J. Ma, Y. Fan, and X. Wu, "Single fiber-type double cavity enhanced photoacoustic spectroscopy sensor for trace methane sensing," *Journal of Lightwave Technology*, 2024, 42(9): 3393–3398.

[27] W. Cheng, H. Zhu, F. Zheng, B. Chu, R. Wang, J. Tao, *et al*., "Phototaxis flight of microdroplets in a laser," *Physical Review Letters*, 2024, 132(10): 104001.

[28] X. Tu, C. Qian, T. Feng, Y. Zhen, B. Cui, T. Li, *et al*., "Insect-inspired micro-optical antenna enables ultrasensitive multisensory perception," *Science Advances*, 2025, 11(50): eaec4252.

[29] K. Pearson, "On lines and planes of closest fit to systems of points in space," *The London, Edinburgh, and Dublin Philosophical Magazine and Journal of Science*, 1901, 2(11): 559–572.

[30] Y. Freund and R. E. Schapire, "A decision-theoretic generalization of on-line learning and an application to boosting," *Journal of Computer and System Sciences*, 1997, 55(1): 119–139.

[31] J. L. Johnson, M. Merrilees, J. Shragge, and K. van Wijk, "All-optical extravascular laser-ultrasound and photoacoustic imaging of calcified atherosclerotic plaque in excised carotid artery," *Photoacoustics*, 2018, 9: 62–72.

[32] J. L. Johnson, J. Shragge, and K. van Wijk, "Nonconfocal all-optical laser-ultrasound and photoacoustic imaging system for angle-dependent deep tissue imaging," *Journal of Biomedical Optics*, 2017, 22(4): 041014.

[33] Y. Bian, R. Zheng, F. P. Bayer, C. Wong, Y. C. Chang, C. Meng, *et al*., "Robust, reproducible and quantitative analysis of thousands of proteomes by micro-flow LC-MS/MS," *Nature Communications*, 2020, 11(1): 157.

[34] Z. Wang, K. Wang, Q. Han, J. Ni, and Z. Wu, "Crack imaging of underwater concrete components using interfacial waves and transducer array," *Mechanical Systems and Signal Processing*, 2025, 224: 111998.

[35] Z. Meng, W. Chen, J. Wang, X. Hu, M. Chen, and Y. Zhang, "Recent progress in fiber-optic hydrophones," *Photonic Sensors*, 2021, 11(1): 109–122.

[36] S. Das, R. Devireddy, and M. R. Gartia, "Surface plasmon resonance (SPR) sensor for cancer biomarker detection," *Biosensors*, 2023, 13(3): 396–428.

[37] C. L. Zhang, Y. Q. Wang, Y. Gong, Y. Wu, G. D. Peng, and Y. J. Rao, "The generation and assembly of laser-induced microbubbles," *Journal of Lightwave Technology*, 2018, 36(12): 2492–2498.

[38] R. Wang, H. Zhang, Q. Liu, F. Liu, X. Han, X. Liu, *et al*., "Operando monitoring of ion activities in aqueous batteries with plasmonic fiber-optic sensors," *Nature Communications*, 2022, 13(1): 547.

[39] J. Liu, M. Osadchy, L. Ashton, M. Foster, C. J. Solomone, and S. J. Gibson, "Deep convolutional neural networks for Raman spectrum recognition: a unified solution," *Analyst*, 2017, 21(142): 4067–4074.

[40] J. Wäldchen and P. Mäder, "Machine learning for image based species identification," *Methods in Ecology and Evolution*, 2018, 9: 2216–2225.